applied sciences

MDPI

Article

Vehicle Cornering Performance Evaluation and Enhancement Based on CAE and Experimental Analyses

Hsing-Hui Huang * and Ming-Jiang Tsai

Department of Vehicle Engineering, National PingTung University of Science and Technology, Pingtung County 91201, Taiwan; k199079719@gmail.com

* Correspondence: sanlyhuang@mail.npust.edu.tw

Received: 14 October 2019; Accepted: 4 December 2019; Published: 11 December 2019

check for updates

Featured Application: Measurement and performance evaluation for vehicle.

Abstract: A full-vehicle analysis model was constructed incorporating a SLA (Short Long Arm) strut front suspension system and a multi-link rear suspension system. CAE (Computer Aided Engineering) simulations were then performed to investigate the lateral acceleration, yaw rate, roll rate, and steering wheel angle of the vehicle during constant radius cornering tests. The validity of the simulation results was confirmed by comparing the computed value of the understeer coefficient (K_{us}) with the experimental value. The validated model was then used to investigate the steady-state cornering performance of the vehicle (i.e., the roll gradient and yaw rate gain) at various speeds. The transient response of the vehicle was then examined by means of simulated impulse steering tests. The simulation results were confirmed by comparing the calculated values of the phase lag, natural frequency, yaw rate gain rate, and damping ratio at various speeds with the experimental results. A final series of experiments was then performed to evaluate the relative effects of the cornering stiffness, initial toe-in angle, and initial camber angle on the steady-state and transient-state full-vehicle cornering handling performance. The results show that the handling performance can be improved by increasing the cornering stiffness and initial toe-in angle or reducing the initial camber angle.

Keywords: vehicle suspension system; vehicle cornering performance; understeer coefficient; yaw rate gain; CAE analyses

1. Introduction

The dynamic handing performance of a vehicle is one of the most important aspects affecting driving safety. The chassis system of a vehicle consists of three major subsystems, namely, the suspension system, the steering system, and the brake system. Generally speaking, a superior handling quality indicates that the vehicle reaches the motion state required by the driver more accurately and rapidly, while a superior stability indicates that the vehicle is able to rapidly restore the original motion state under external interference when it is running. In practice, the handling quality and vehicle stability are closely related to one another and are fundamentally dependent on the effectiveness of the suspension and steering systems. Consequently, a proper understanding and design of the various parameters associated with the two systems is essential.

Computer Aided Engineering (CAE) technology has matured rapidly in recent years and is now used extensively throughout the automobile industry to evaluate and predict the full-vehicle dynamic behavior during the design, development, and prototype stages. Compared to traditional experimental methods, CAE simulations yield a significant reduction in the time and cost of the development process. For example, Holdmann et al. [1] used ADAMS (Automated Dynamic Analysis of Mechanical Systems) software to conduct the simulated kinematics and compliance testing of a virtual suspension system prior to conducting physical experiments.

Dixon [2] presented an analytical approach based on Ackerman theory for analyzing and controlling five critical suspension properties, namely, the bump steer, the roll steer, the bump camber, the compliance steer, and the roll center. Mitchell et al. [3] examined the use of two different measurements for optimizing the Ackermann steering geometry and proposed a single formula for relating the two. Wang et al. [4] analyzed the relationship between the inside and outside steered wheels of an automobile and used the experimental results to correct the theoretical equation for the Ackerman steering angle such that the actual steering angle more closely approached the calculated value. Upadhyay et al. [5] examined the effects of the steering geometry, steering system compliance, steering linkage friction, and tire static friction torque on the steering effort in commercial vehicles. A methodology was then proposed for fine tuning the design and dimensions of the steering linkages in such a way as to minimize the steering effort while satisfying the imposed constraints on the hardpoints. Singh et al. [6] examined the effects of dynamic load variations on the steering geometry of a vehicle and the resulting non-uniform tire wear of the front steered wheels. Azasi and Mirzadeh [7] used ADAMS software to investigate the effects of changes in the steering hardpoint positions on the full-vehicle motion characteristics of a passenger car. The sensitivity results were then used to optimize the steering system parameters that will help vehicles with the integration of individual modular chassis control systems in order to provide key advantages for vehicle power such as AFS (Adaptive Front-Lighting System), 4WD (4-Wheel Drive), ECS (electronic control suspension system). It seems to be a more efficient method to provide crucial benefits for vehicle dynamics such as agility, maneuverability or additional stability improvement [8–11].

The present study conducts a numerical and experimental investigation into the cornering handling performance of a commercial vehicle incorporating a SLA (Short Long Arm) strut front suspension system and a multi-link rear suspension system. A full-vehicle analysis model was constructed and used in a series of CAE simulations to investigate the steady-state and transient-state response of the vehicle handling performance during constant radius cornering tests and impulse steering tests, respectively. The validity of the steady-state simulation results was demonstrated by comparing the calculated value of the understeer coefficient with the experimental value. Similarly, the validity of the transient-state simulations was demonstrated by comparing the simulated four-parameter radar plots (i.e., phase lag, natural frequency, yaw rate gain, and damping ratio [12]) with the experimental plots. Finally, the validated simulation model was used to explore the relative effects of three suspension design variables (namely, the cornering stiffness, the initial toe-in angle, and the initial camber angle [13]) on the full-vehicle cornering handling performance.

2. Method and Modeling

Figure 1 presents a flowchart of the research framework employed in the present study. The study commenced by collecting the design parameters of the suspension and steering systems of the target vehicle. Based on the hardpoint measurements of the vehicle, a half-vehicle model was constructed comprising the front and rear suspension systems and the steering system. The validity of the half-model was confirmed experimentally, and a full-vehicle analysis model was then constructed. Simulations were performed to investigate the steady-state and transient-state cornering handling performance of the vehicle under typical driving maneuvers. The simulation results were validated experimentally. The validated model was then used to investigate the effects of three main suspension design parameters on the cornering performance.

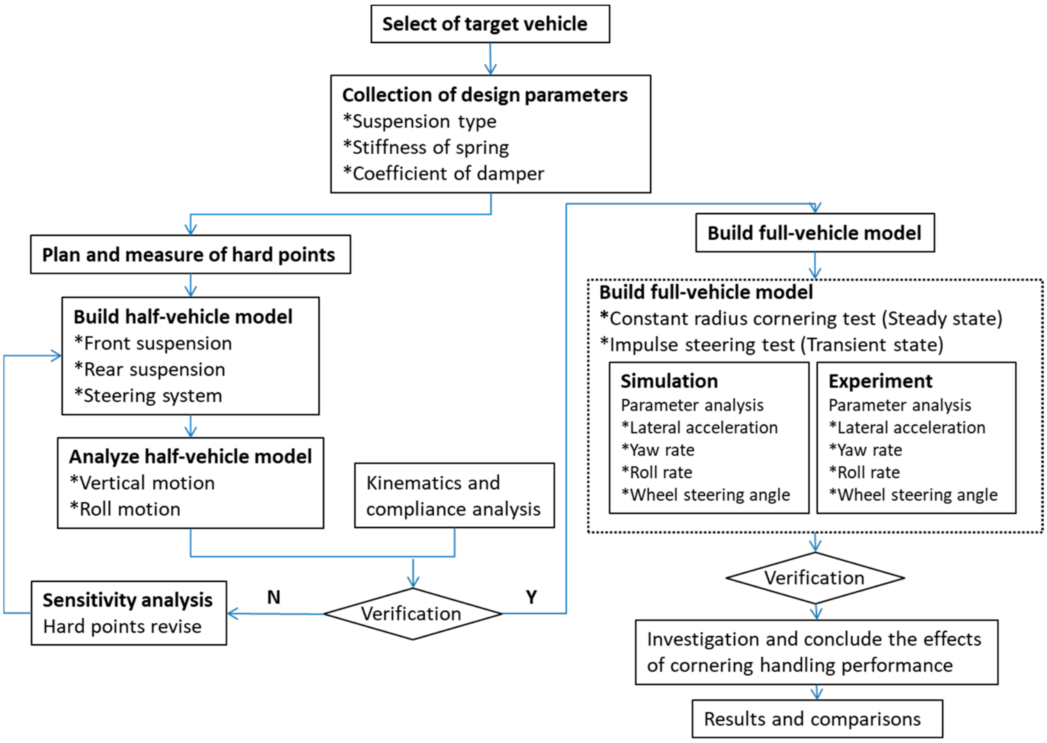

Figure 1. Research framework.

As shown in Figure 2, the target vehicle was fitted with an SLA Strut front suspension system and a multi-link rear suspension system. Referring to the two degree-of-freedom (2-DOF) model shown in Figure 3, the equations of motion for the vehicle can be derived as Equation (1):

$$
\begin{aligned}
m(\dot{V}_x - V_y\Omega_z) &= F_{xf}\cos\delta_f + F_{xr} - F_{yf}\sin\delta_f \\
m(\dot{V}_y - V_x\Omega_z) &= F_{yf}\cos\delta_f + F_{yr} - F_{xf}\sin\delta_f \\
I_z\dot{\Omega}_z &= l_1F_{yf}\cos\delta_f - l_2F_{yr} + l_1F_{xf}\sin\delta_f
\end{aligned}
\quad (1)
$$

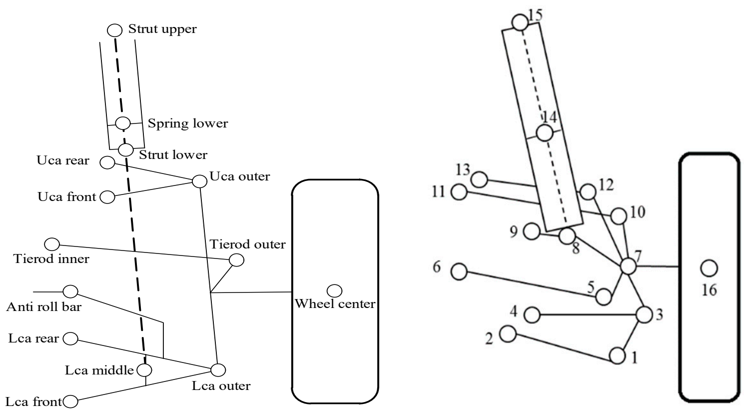

(**a**) (**b**)

Figure 2. Hardpoint positions in the front and rear suspension systems. (**a**) Hardpoint positions in the SLA strut suspension; (**b**) hardpoint positions in the multi-link suspension.

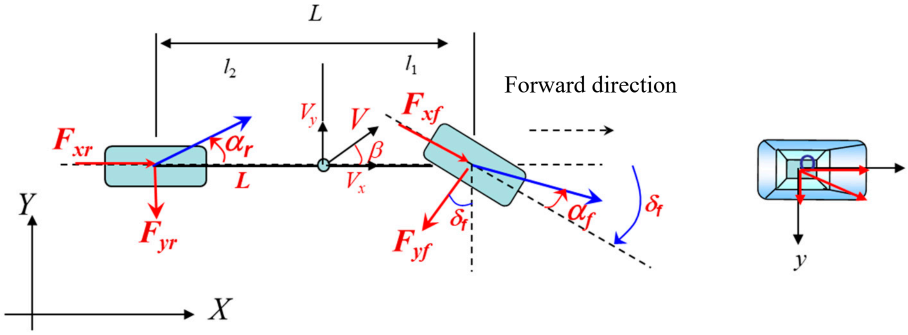

Figure 3. Body-centered axis model.

For reasons of simplicity, the following assumptions are introduced: (1) the longitudinal acceleration of the whole vehicle is equal to zero, and (2) the longitudinal traction force is also equal to zero, i.e., $F_{xf} \approx 0$. Furthermore, the steer angle (δ_f) of the tire is small, i.e., $\cos\delta_f \approx 1$. Consequently, the equations of motion can be simplified as:

$$m(\dot{V}_y - V_x\Omega_z) = F_{yf} + F_{yr}$$
$$I_z\dot{\Omega}_z = l_1F_{yf} - l_2F_{yr}$$

Notably, the two equations above describe the dynamic response of the vehicle under turning irrespective of the roll motion of the body or the angles of the various wheel alignments.

Considering the tire forces developed at each wheel of the vehicle, the tire slip angles at the front and rear can be expressed respectively as:

$$\alpha_f = \delta_f - \frac{l_1\Omega_z + V_y}{V_x}$$
$$\alpha_r = \frac{l_2\Omega_z - V_y}{V_x}$$

Let the front and rear cornering stiffnesses be denoted as $C_{\alpha f}$ and $C_{\alpha r}$, respectively. The tire forces at the front and rear can then be derived as:

$$F_{yf} = 2C_{\alpha f}\alpha_f;\ F_{yr} = 2C_{\alpha r}\alpha_r$$

Let $\tan\beta = \frac{V_x}{V_y} \cong \beta$, such that $V_y \cong \beta V_x$ and $\dot{V}_y \cong \beta\dot{V}_x + \dot{\beta}V_x$.

Assuming that angle β is very small, then $\tan\beta = \beta$, V_x is constant, $\dot{V}_x$ is zero, and $\dot{V}_y = \dot{\beta}V_x$. Furthermore, if the vehicle maintains a constant speed as it turns, the overall vehicle dynamic behavior can be expressed as:

$$m\dot{V}_y + \left[mV_x + \frac{2l_1C_{\alpha f} - 2l_2C_{\alpha r}}{V_x}\right]\Omega_z + \left[\frac{2C_{\alpha f} + 2C_{\alpha r}}{V_x}\right]V_y = 2C_{\alpha f}\delta_f$$
$$I_z\dot{\Omega}_z + \left[mV_x + \frac{2l_1^2C_{\alpha f} - 2l_2^2C_{\alpha r}}{V_x}\right]\Omega_z + \left[\frac{2l_1C_{\alpha f} - 2l_2C_{\alpha r}}{V_x}\right]V_y = 2l_1C_{\alpha f}\delta_f$$

The tendency of a vehicle to steer less than the amount commanded by the driver during steady-state curve maneuvers can be evaluated using the understeer coefficient (K_{us}). Three methods are available for computing K_{us}, namely:

Method 1:

$$K_{us} = \frac{\alpha_f - \alpha_r}{A_y}$$

where $\alpha_f = (\alpha_{Lf} + \alpha_{Rf})/2$ and $\alpha_r = (\alpha_{Lr} + \alpha_{Rr})/2$.

Method 2:

$$K_{us} = \frac{ang_{act} - ang_{in}}{A_y}$$

where ang_{act} is the (steering wheel angle)/(overall steering ratio), and is given as:

$$ang_{in} = \frac{L \times A_y}{V_x^2} = L \times \frac{V_x^2}{R} \times \frac{1}{V_x^2} = \frac{L}{R}$$

In addition, ang_{in} is the Ackerman steering angle and is given theoretically as:

$$\theta = \tan^{-1}\frac{L}{R} \approx \frac{L}{R}$$

Method 3: Bicycle model

$$Kus = \frac{W_f}{C_{\alpha f}} - \frac{W_r}{C_{\alpha r}}$$

Among these three methods, Methods 1 and 2 are simple and extensively applied, and Method 3 is tenable if the speed is very low and no lateral acceleration or slip angle occurs [14,15]. In the present study, the steady-state analysis considered a low-speed curve maneuver (10 km/h). Hence, Method 3 was used to compute the understeer coefficient.

3. Vehicle Experimental Equipment and Method

In examining the cornering handling performance of the target vehicle, the present study considered both the steady-state cornering characteristics and the transient-state characteristics as evaluated in constant radius cornering tests and impulse steering tests, respectively. For both tests, the simulation results were confirmed by comparison with the experimental results.

3.1. Experimental Equipment

Figure 4 illustrates the experimental platform used in the present study including the target vehicle, V-Box host, gyroscope, steering effort sensor, and GPS antenna.

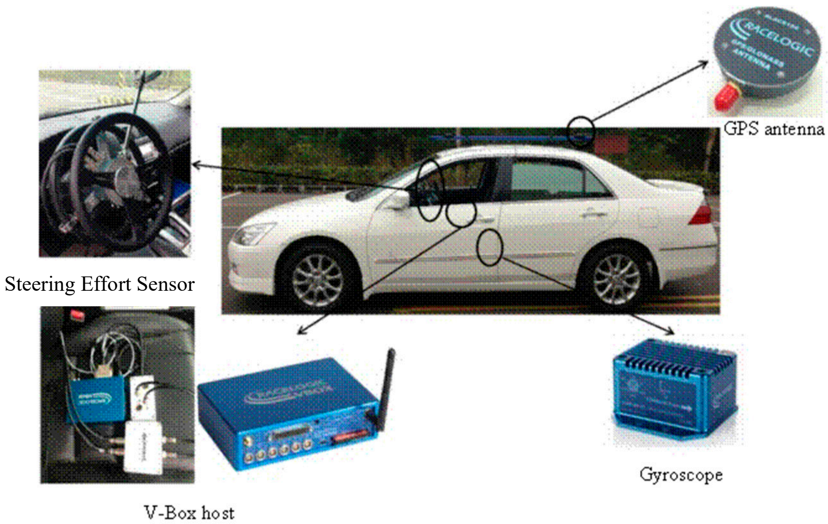

Figure 4. Experimental platform for full vehicle dynamics.

3.2. Constant Radius Cornering Test

The vehicle cornering behavior is an important component of the overall vehicle handling performance. In real driving conditions, the driver and vehicle form a closed-loop system, in which the driver observes the vehicle response and adjusts the command parameters accordingly in order to correct the vehicle response so as to obtain the desired behavior. However, to determine the true steady-state behavior of the vehicle under cornering, it is necessary to perform open-loop experiments free of driver correction. In the present study, this was achieved by means of simulated and experimental constant radius cornering tests with the understeer coefficient, K_{us}, taken as the performance metric.

3.3. Impulse Steering Test

The impulse steering test evaluates the transient-state response of a vehicle during cornering at a constant speed set at approximately 70% of the maximum speed. In performing the test, a Gaussian pulse steering angle was applied to the steering wheel, and, when the preset lock angle was reached, the wheel was returned quickly (within 0.5 s) to the origin and then held still as the vehicle continued straight running in the forward direction (see Figure 5). The vehicle speed, steering wheel angle, yaw rate, and lateral acceleration were recorded continuously during the testing process, and the corresponding acceleration gain and yaw rate gain were then converted into the frequency domain by Fourier transform as shown in Figure 6. The transfer functions of the lateral acceleration gain (G_{acc}) and yaw rate gain (G_{yaw}) were obtained by system parameter identification. Finally, the vehicle handling responsiveness was visualized using four-parameter radar plots based on the phase lag, natural frequency, yaw rate gain, and damping rate, respectively [12].

Figure 5. Schematic illustration of impulse steering test.

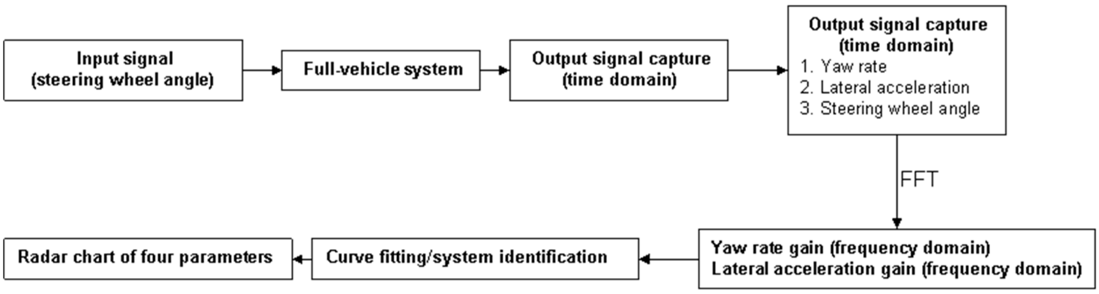

Figure 6. Impulse steering test measurement and analysis process. (FFT: Fast Fourier Transform).

4. Model Verification

4.1. Constant Radius Cornering Tests

The validity of the full-vehicle model was investigated firstly by comparing the calculated value of the understeering coefficient, K_{us}, during a simulated constant radius cornering test with the value determined experimentally. The test was performed at a low speed of 10 km/h with a constant steering wheel angle set in such a way as to achieve a turn radius of 30 m. The steering wheel angle, speed, and lateral acceleration were computed (simulation study) and measured (experimental study), and the understeering coefficients, K_{us}, were then calculated using Method 3. The corresponding results are presented in Table 1. As shown, the experimental and simulated values of K_{us} were 4.68 and 5.15, respectively. The discrepancy between the two values was due most likely to the rigid-body assumption made in the simulation model for the cornering subsystem components, compared to the flexibility of the actual components in the real-world system. However, the simulated value of K_{us} deviated from the experimental value by less than 10%. Hence, the validity of the full-vehicle analysis model for evaluating the steady-state cornering response of the vehicle was confirmed.

Table 1. Experimental and simulation results for K_{us} in constant radius cornering tests.

Experimental Data			
Speed (km/h)	Tire steering angle (degree)	Lateral acceleration (G)	K_{us} (rad/g)
10	12.9	0.048	4.68
CAE model Data			
Speed (km/h)	Tire steering angle (degree)	Lateral acceleration (G)	K_{us} (rad/g)
10	9.47	0.032	5.15

The validated model was used in a further series of simulations to investigate the roll gradient and yaw rate gain of the vehicle when driving a circular path with a radius of 50 m at constant speeds of 10–80 km/h, corresponding to lateral accelerations in the range of 0.01 G to 0.4 G.

4.1.1. Roll Gradient

The roll gradient is defined as the ratio of the roll angle to the lateral acceleration and is one of the most common steady-state cornering performance indicators for a vehicle. An excessive roll angle degrades the vehicle stability, and hence limits the ability of the driver to respond to any contingencies when steering around the corner. In extreme cases, the vehicle may even overturn. By contrast, a small roll angle increases the vehicle turning radius therefore minimizing the load transfer under cornering and reducing the off-side wheel grip ability. As a result, the vehicle is likely to yaw thereby degrading the full-vehicle handling performance. Table 2 shows the simulation results obtained for the roll gradient at different speeds. In general, the results show that the roll gradient increased non-linearly with an increasing lateral acceleration. As such, they provide an important reference for predicting the vehicle roll angle at different speeds and enhancing the driving predictability and safety as a result.

Table 2. Simulation results for roll gradient at different speeds.

Velocity (km/h)	**Lateral Acceleration (G)**	**Roll Angle (°)**	**Roll Gradient (°/g)**
10	0.018	0.046	2.56
20	0.064	0.17	2.65
30	0.165	0.45	2.72
40	0.252	0.7	2.78
50	0.393	1.13	2.87

4.1.2. Yaw Rate Gain

As a vehicle corners, or undergoes certain lateral tilting motions, a yaw effect is induced in which the vehicle performs rotary angular movement around the vertical axis. For general vehicles, the yaw rate (i.e., the angular velocity of yaw) varies linearly with the steering wheel angle during cornering at low speeds. However, to ensure driving comfort and safety, the yaw rate should be suppressed as the cornering speed increases. Together with the roll gradient, the steady-state yaw rate gain (defined as the ratio of the yaw rate to the front wheel angle) is one of the most important measures for evaluating the cornering performance of a vehicle. Figure 7 shows the simulation results obtained for the yaw rate gain of the present vehicle at speeds in the range of 10–80 km/h. At low speeds, the yaw rate gain increases linearly with an increasing vehicle speed. However, as the speed increases beyond 70 km/h, the yaw rate gain decreases, indicating the occurrence of understeer.

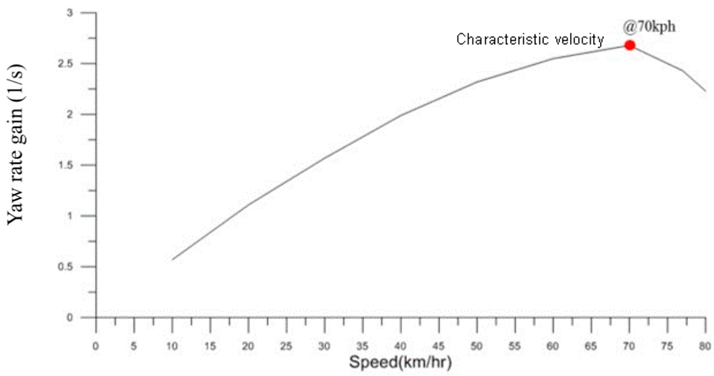

Figure 7. Relationship between yaw rate gain and cornering speed for target vehicle.

Table 3 shows the full-vehicle parameters obtained from the experimental measurement tests for the target vehicle.

Table 3. Full-vehicle parameters.

Designation	Symbol	Unit	Value
Front axle weight	W_f	N	8829
Rear axle weight	W_r	N	5886
Front wheel cornering stiffness	$C_{\alpha f}$	N/rad	78,855.7
Rear wheel cornering stiffness	$C_{\alpha r}$	N/rad	71,687
Pneumatic trail	P	m	0.018754
Wheelbase	L	m	2.8
Steering angle per unit lateral force	q	°/N	1.194×10^{-4}(f)/1.0498×10^{-4}(r)
Roll steer coefficient	ε	°/°	−0.117213(f)/0.02272(r)
Roll angle	$\emptyset$	°	0.7047
Lateral acceleration	A_y	G	0.2521
Camber stiffness	C_γ	N/rad	7885.57(f)/7168.7(r)

Based on the parameters presented in Table 3, the effects of tire stiffness, aligning torque, lateral force compliance steer, roll steer, and roll camber on the understeer coefficient, K_{us}, can be evaluated as follows.

1. Tire Cornering Stiffness

$$Ktires = \frac{W_f}{C_{\alpha f}} - \frac{W_r}{C_{\alpha r}}$$
$$Ktires = \frac{8829}{78{,}855.7} - \frac{5886}{71{,}687} = 1.71^\circ \tag{2}$$

2. Aligning Torque

The vehicle tire generates an aligning torque to resist the cornering. However, the aligning torque produces a lateral force which acts on the pneumatic trail at the contact point behind the tire center and produces an understeer effect. In general, the understeer term is given by:

$$Kat = W\frac{p}{L} - \frac{C_{\alpha f} + C_{\alpha r}}{C_{\alpha f} C_{\alpha r}} \tag{3}$$

When $C_{\alpha f}$ has a positive value, the aligning torque effect of the tire is positive (i.e., understeer). For the target vehicle, the understeer effect is computed as:

$$Kat = 15{,}696 \times \frac{0.018754}{2.8} \times \frac{(78{,}855.7 + 71{,}687)}{78{,}855.7 \times 71{,}687} = 0.16^\circ$$

3. Lateral Force Compliance Steer

When the vehicle performs cornering, the members of the suspension system may undergo lateral deformation. Since the understeer effect is directly correlated with the steering angles of the front and rear axles, respectively, the effect of the compliance steer of the members resulting from the lateral force described above on the understeer can be quantified as:

$$\begin{gathered} K_{lfcs} = q_f W_f - q_r W_r \\ K_{lfcs} = 0.0001194 \times 9417.6 - 0.00010498 \times 6278.4 = 0.465\ (^\circ) \end{gathered} \tag{4}$$

4. Roll Steer

When the vehicle rolls during cornering, the sprung mass results in a weight transfer, which subsequently affects the suspension system. In particular, the wheels undergo a slight steering motion in relation to the sprung mass, resulting in a phenomenon referred to as roll steer. The relationship between the roll steer and the understeer effect can be modeled as:

$$\begin{gathered} K_{rollsteer} = (\varepsilon_f - \varepsilon_r)\frac{d\phi}{d_{ay}} \\ K_{rollsteer} = (-0.117213 - 0.02272) \times \frac{0.7047}{0.2521} = 0.392(^\circ/\mathrm{g}) \end{gathered} \tag{5}$$

5. Roll Camber

The camber angle describes the inclination of the wheel relative to the vehicle body and has a positive value if the wheel is inclined away from the vehicle body and a negative value otherwise. The camber angle generates a force known as the roll camber which is applied from the vehicle body to the wheel and the tire ground point. The roll camber and vehicle understeer are related as follows:

$$\begin{gathered} Kr = \left(\frac{C_{\gamma f}}{C_{\alpha f}}\frac{\partial \gamma f}{\partial \phi} - \frac{C_{\gamma r}}{C_{\alpha f}}\frac{\partial_{\gamma r}}{\partial \phi}\right)\frac{\partial \phi}{\partial ay} \\ Kr = \left(\left(\frac{7885.57}{78855.7}\right) \times 0.8757 - \left(\frac{7168.7}{71687}\right) \times 1.6095\right)\frac{0.7047}{0.2521} = -0.205(^\circ/\mathrm{g}) \end{gathered} \tag{6}$$

Based on the results obtained from Equations (1)–(5), the five parameters described above can be ranked in terms of decreasing influence on the understeer coefficient, K_{us}, as follows: tire stiffness > lateral force compliance steer > roll steer > roll camber > aligning torque.

4.2. Impulse Steering Tests

The transient-state cornering handling performance of the target vehicle was evaluated by means of a simulated impulse steering test performed at a speed of 70 km/h with a steering wheel angle change of 65° (corresponding to a lateral acceleration of approximately 0.4 G) within 0.4 s. As described in Section 3.3, the validity of the simulation results was confirmed by comparing the calculated values of the phase lag, natural frequency, yaw rate gain, and damping ratio with the experimental values (see Table 4). For ease of visualization and comparison, the two sets of data were also presented as four-parameter radar charts, as shown in Figure 8, in which the vehicle transient handling performance is represented by the area and position of the enclosed diamond region of the chart.

Table 4. Experimental and simulation results for the impulse steering tests.

Experimental Data				
Speed (km/h)	Phase lag (ϕ) (deg)	Natural frequency (fn) (Hz)	Yaw rate gain (a1) (1/s)	Damping ratio (ζ)
70	−36.81	1.9567	0.24618	0.5581
CAE model Data				
Speed (km/h)	Phase lag (ϕ) (deg)	Natural frequency (fn) (Hz)	Yaw rate gain (a1) (1/s)	Damping ratio (ζ)
70	−26	1.8825	0.18099	0.94961

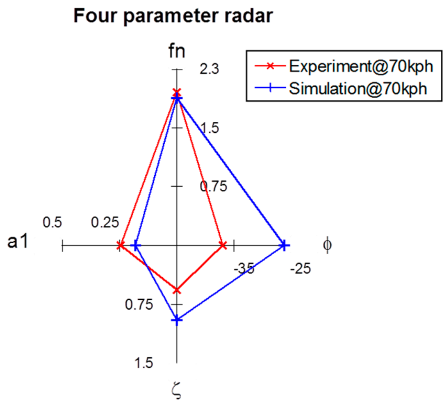

Figure 8. Experimental and simulated four-parameter radar charts for the impulse steering tests.

Observation of Figure 8 shows a good quantitative agreement between the experimental and simulation results for the natural frequency (fn) and steady-state yaw rate gain (a1). However, an obvious difference exists between the two sets of results for the damping ratio (ζ) and phase lag (ϕ). As described earlier in Section 4.1 for the constant radius cornering test, this discrepancy arises since the CAE model is based on a rigid-body assumption, whereas the linkages, bushes, bearings, racks, and tires in the actual vehicle system are compliant. Nonetheless, a good qualitative agreement was observed between the two radar plots, and, hence, the basic validity of the simulation model was confirmed.

To further evaluate the transient handling response of the vehicle, additional simulated impulse steering tests were performed at speeds ranging from 40–120 km/h. The corresponding results for the phase lag, natural frequency, steady-state yaw rate gain, and damping ratio are shown in Table 5. In addition, the four-parameter radar plots are presented in Figure 9. In general, the size of the enclosed diamond area of the radar plots reduced with increasing vehicle speed, indicating a degradation of the vehicle handling performance. This tendency is consistent with the real-world situation, and, hence, the validity of the CAE model was once again confirmed. Overall, the results presented in Table 5 support the following major conclusions:

Table 5. Simulation results for impulse steering tests performed at different speeds.

Speed (km/h)	Phase Lag (ϕ) (deg)	Natural Frequency (fn) (Hz)	Yaw Rate Gain (a1) (1/s)	Damping Ratio (ζ)
40	−1.849	2.3739	0.134	1.62
70	−26	1.8825	0.18099	0.94961
80	−26.9	1.8624	0.18402	0.91857
90	−29.49	1.8544	0.18454	0.84993
100	−31.98	1.7871	0.1854	0.7842
120	−34.96	1.6747	0.18278	0.69063

Yaw rate gain (a1): a1 represents the yaw rate gain in the steady state. Therefore, at speeds below the characteristic speed of the vehicle (70 km/h, see Figure 7), the yaw rate gain had a relatively low value. However, as the speed reached and then surpassed the characteristic speed, the yaw rate increased significantly and then remained approximately constant.

Natural frequency (fn): fn quantifies the immediacy of the steering response in terms of the relationship between the steering wheel angle and the yaw rate. To generate the required 0.4 G lateral acceleration, the steering wheel angle decreased as the speed increased. Therefore, the natural frequency also decreased gradually with an increasing vehicle speed.

Damping ratio (ζ): ζ represents the ratio of the steady-state yaw rate gain to the transient yaw rate gain, where a higher value of ζ indicates an improved nose convergence. According to the results presented in Table 5, the damping ratio decreased with an increasing speed. In other words, the nose convergence worsened as the speed increased, indicating a higher risk of vehicle instability.

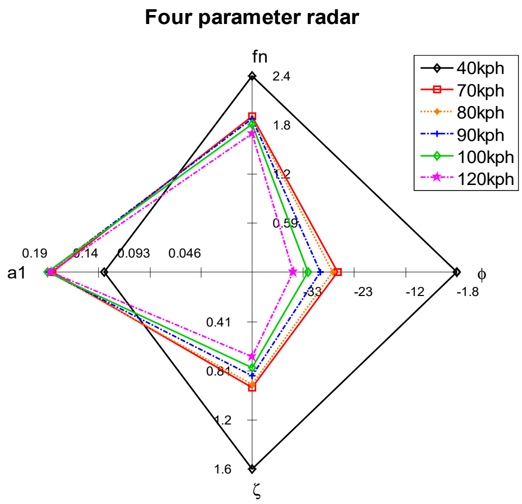

Figure 9. Simulated four-parameter radar charts for impulse steering tests performed at different speeds.

Phase lag (ϕ): ϕ represents the phase lag angle at a 1 Hz lateral acceleration. A smaller value of ϕ represents a better handling performance in emergency cornering. For a low speed of 40 km/h, the phase lag had a low value of −1.849. However, as the vehicle speed increased, the phase lag increased significantly. In other words, as expected, the handling performance and stability were degraded as the vehicle speed increased.

5. Discussions

As described in Section 4.1, for the target vehicle considered in the present study, the chassis system factors affecting the understeer coefficient, K_{us}, can be ranked in order of decreasing effect as follows: tire stiffness > lateral force compliance steer > roll steer > roll camber > aligning torque. This section performs a further detailed investigation into the effects of the cornering stiffness, roll steer, and roll camber on the understeer behavior of the vehicle with the aim of identifying the parameter settings which optimize the vehicle cornering handling performance.

5.1. Cornering Stiffness

In tire motion analysis, the tire characteristics are affected by numerous factors, including the tire size, the tire tread, the rubber material, the working temperature, and the road surface roughness. In the present analysis, the cornering stiffness was assigned three different types, namely, Type 1: the original cornering stiffness; Type 2: the original cornering stiffness increased by 30%; and Type 3: the original cornering stiffness reduced by 30% (see Table 6). Figure 10 compares the simulation results obtained for the variation of the lateral force with the tire slip angle for the three different cornering stiffness values.

Table 6. Cornering stiffness values.

Item	Cornering Stiffness (N/rad)
Type 1 (original)	71,687
Type 2 (increased by 30%)	93,193.1
Type 3 (decreased by 30%)	50,180.9

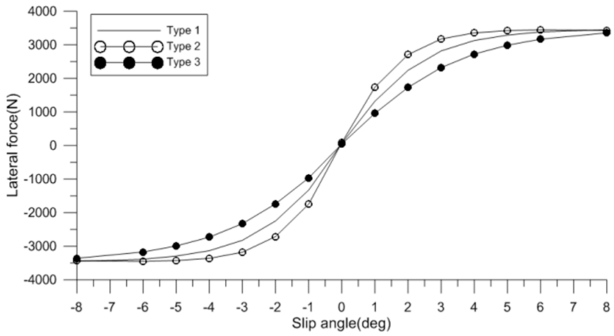

Figure 10. Variation of lateral force with tire slip angle for three different cornering stiffness values.

5.1.1. Constant Radius Cornering Test: Understeer Coefficient (Steady-State Response)

Simulated constant radius cornering tests were performed at speeds of 20–80 km/h using the three different values of the cornering stiffness defined in Table 6. For each test, the understeer coefficient, K_{us}, was calculated using Method 3, as described earlier. The corresponding results are presented in Table 7 and Figure 11.

Table 7. Understeer coefficients computed at different vehicle speeds using different cornering stiffness values.

Velocity (km/h)	K_{us} (Type 1) (rad/g)	K_{us} (Type 2) (rad/g)	K_{us} (Type 3) (rad/g)
20	1.560	1.534	1.598
30	0.734	0.705	0.776
40	0.443	0.414	0.486
50	0.306	0.275	0.348
60	0.232	0.201	0.272
70	0.190	0.158	0.230
77	0.194	0.151	0.235
80	0.204	0.168	0.255

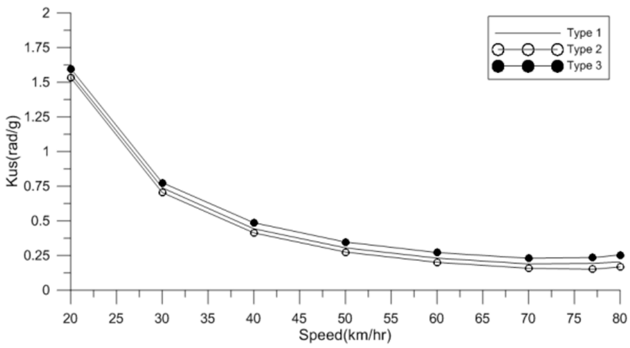

Figure 11. Variation of understeer coefficient with vehicle speed for three different cornering stiffness values.

As the cornering stiffness decreases, the tire slip angle intuitively increases. To maintain a constant turning radius, the steering wheel angle must therefore be increased. Consequently, the understeer coefficient of the tire also increases. In other words, for a given speed, the effects of the different cornering stiffness values on the understeer coefficient are ranked as follows: Type 3 > Type 1 > Type 2.

5.1.2. Constant Radius Cornering Test: Yaw Rate Gain (Steady-State Response)

Table 8 and Figure 12 show the simulation results obtained for the yaw rate gain at vehicle speeds in the range of 10–80 km/h and the three different tire cornering stiffness values.

Table 8. Yaw rate gain computed at different vehicle speeds using three different cornering stiffness values.

Velocity (km/h)	Yaw Rate Gain (Type 1) (1/s)	Yaw Rate Gain (Type 2) (1/s)	Yaw Rate Gain (Type 3) (1/s)
10	0.57	0.57	0.57
20	1.11	1.13	1.08
30	1.57	1.65	1.50
40	1.99	2.14	1.82
50	2.32	2.57	2.04
60	2.55	2.93	2.17
70	2.68	3.22	2.21
77	2.43	3.12	2.00
80	2.23	2.69	1.78

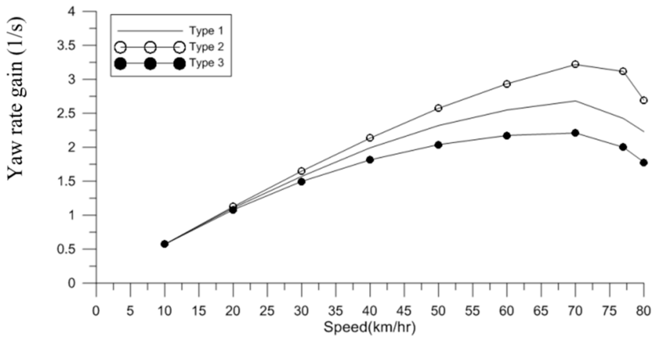

Figure 12. Variation of yaw rate gain with vehicle speed for three different cornering stiffness values.

As shown in Figure 12, the yaw rate gain for the Type 2 cornering stiffness was higher than that for the Type 1 (original) or Type 3 (lower) cornering stiffness. In other words, given a constant lateral force acting on the tire, a higher cornering stiffness improves the steering sensitivity (i.e., reduces the tire slip angle) and enhances the handing performance as a result.

5.1.3. Impulse Steering Tests: Four-Parameter Radar Plots (Transient-State Response)

Figure 13 and Table 9 show the simulation results obtained for the phase lag, natural frequency, steady-state yaw rate gain, and damping ratio in impulse steering tests performed using the three different values of the cornering stiffness. In general, the transient response of the vehicle during the impulse steering tests can be quantified using the full-vehicle stability factor, K, defined as [12]:

$$K = \frac{m(l_2 C_{\alpha r} - l_1 C_{\alpha f})}{2L^2 C_{\alpha f} C_{\alpha r}}$$

where m is the vehicle mass; l_2 is the distance between the full-vehicle center of gravity and the rear axle; l_1 is the distance between the full-vehicle center of gravity and the front axle; $C_{\alpha f}$ and $C_{\alpha r}$ are the front wheel cornering stiffness and rear wheel cornering stiffness, respectively; and L is the full-vehicle wheel base.

Table 9. Simulation results for impulse steering tests performed using different cornering stiffness values.

Item	Phase Lag (ϕ) (deg)	Natural Frequency (fn) (Hz)	Yaw Rate Gain (a1) (1/s)	Damping Ratio (ζ)
Type 1	−26	1.8825	0.18099	0.94961
Type 2	−27.1621	0.89756	0.19171	1.7917
Type 3	−23.08	2.0994	0.14356	0.86539

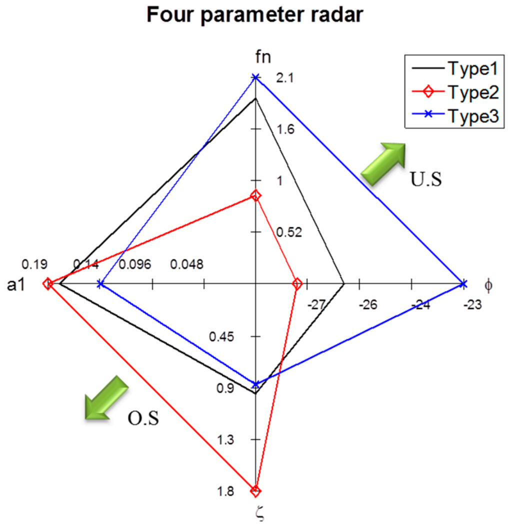

Figure 13. Simulated four-parameter radar charts for impulse steering tests performed using different cornering stiffness values.

As seen in Figure 13, the vehicle tended to oversteer compared to the original vehicle when the Type 2 cornering stiffness was employed since, according to Equation (7), when $C_{\alpha f} > C_{\alpha r}$, the stability factor, K, was smaller than the original value, or was less than zero. According to Tetsushi Mimuro [12], the values of a1 and ζ all increase as K decreases whereas fn decreases. Overall, the results presented in Table 9 and Figure 13 support the following conclusions.

Yaw rate gain (a1): As described previously, the yaw rate gain is the ratio of the yaw rate to the steering wheel angle. The steering wheel angle decreases as the cornering stiffness increases. Hence, the yaw rate gain also increases. Consequently, the relative effects of the cornering stiffness on the yaw rate can be ranked as follows: Type 2 > Type 1 > Type 3.

Natural frequency (fn): The natural frequency describes the relationship between the steering wheel angle and the yaw rate. For a low cornering stiffness, the steering angle needed to obtain the required 0.4 G lateral acceleration increases. Consequently, the natural frequency also tends to increase. As a result, the relative effects of the cornering stiffness on the natural frequency can be ranked as follows: Type 3 > Type 1 > Type 2.

Damping ratio (ζ): The damping ratio is defined as the ratio of the steady-state yaw rate gain to the transient yaw rate gain, where a higher value of ζ indicates an improved nose convergence. In terms of the steady-state gain, the Type 2 cornering stiffness has a greater effect on the damping ratio than the Type 3 stiffness. Consequently, overall, the effects of the cornering stiffness on the damping ratio can be ranked as follows: Type 2 > Type 1 > Type 3.

Phase lag (ϕ): The phase lag is defined as the phase lag angle of the lateral acceleration at 1 Hz. For a low wheel cornering stiffness (Type 3), the slip angle is large, and, hence, the steering wheel angle required to achieve the desired 0.4 G lateral acceleration is larger than that for the Type 1 cornering stiffness. Consequently, the rate of change of the steering wheel angle is also higher, and, hence, the phase lag is reduced. Overall, therefore, the effects of the cornering stiffness on the phase lag can be ranked as follows: Type 3 > Type 1 > Type 2.

5.2. Roll Steer

The roll steer is defined as the slight steering motion of the wheels in relation to the vehicle body when the vehicle rolls during cornering. Geometrically, the roll steer describes the ratio of the variation per unit body roll angle to the variation of the toe-in angle. Accordingly, in seeking to improve the handling performance of the target vehicle, the present analysis considered three different toe-in angles, namely, Type 4 (−1°), Type 5 (0°), and Type 6 (1°) as shown in Table 10.

Table 10. Toe-in angle design variables.

Item	Type 4	Type 5	Type 6
Toe angle (°)	−1	0	1

5.2.1. Constant Radius Cornering Test: Yaw Rate Gain (Steady-State Response)

Figure 14 shows the simulation results obtained for the variation of the yaw rate gain with the vehicle speed given the use of the three different initial toe-in angles. Table 11 shows the detailed analysis results. In general, the results show that the yaw rate gain increases with an increasing toe-in angle.

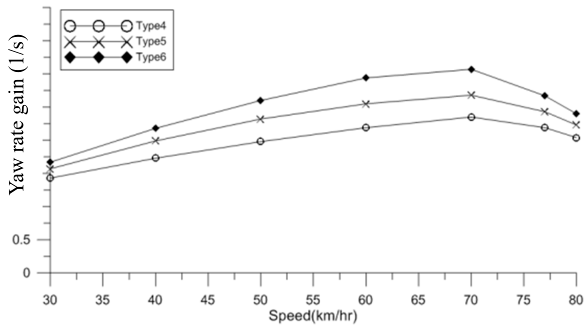

Figure 14. Variation of yaw rate gain with vehicle speed for different initial toe-in angles.

Table 11. Yaw rate gain computed at various vehicle speeds using three different toe-in angles.

Velocity (km/h)	Yaw Rate Gain (Type 4) (1/s)	Yaw Rate Gain (Type 5) (1/s)	Yaw Rate Gain (Type 6) (1/s)
30	1.43	1.57	1.67
40	1.73	1.99	2.18
50	1.98	2.32	2.6
60	2.19	2.55	2.94
70	2.35	2.68	3.07
77	2.18	2.43	2.67
80	2.04	2.23	2.40

Figure 15 presents a schematic illustration showing the effect of the toe-in angle on the lateral force when cornering. As the vehicle steers around a corner, the normal force and lateral force acting on the off-side wheel gradually increase as a result of load transfer. For a smaller slip angle (e.g., 5°), the normal force and lateral force both increase linearly. The lateral force acts behind the wheel center, and, hence, when the toe angle is positive, the lateral force on the outside wheel increases the toe-in angle of the inside wheel. As a result, the lateral force increases the slip angle of the outside wheel. In addition, the nearside wheel slip angle decreases. Therefore, the steering wheel angle also decreases. Consequently, the yaw rate gain increases, and the cornering handling performance is correspondingly improved.

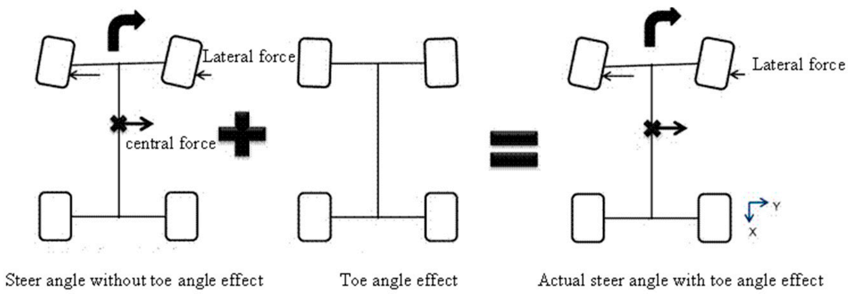

Figure 15. Schematic illustration showing the relationship between toe-in angle and lateral force.

5.2.2. Impulse Steering Test: Four-Parameter Radar Plots (Transient-State Response)

Table 12 and Figure 16 show the simulation results obtained for the phase lag, natural frequency, steady-state yaw rate gain, and damping ratio of the vehicle in impulse steering tests performed using the three different values of the initial toe-in angle. It can be seen that the toe-in angle had only a minor effect on the natural frequency and damping ratio. However, the phase lag and steady-state yaw rate gain exhibited a more significant change as the toe-in angle increased.

Table 12. Simulation results for impulse steering tests performed using different toe-in angles.

Item	Phase Lag (ϕ) (°)	Natural Frequency (fn) (Hz)	Steady-State Gain (a1) (1/s)	Damping Ratio (ζ)
Type 4	−24.88	1.9432	0.15898	0.9656
Type 5	−26	1.8825	0.18099	0.94961
Type 6	−25.5408	1.8106	0.1871	0.96911

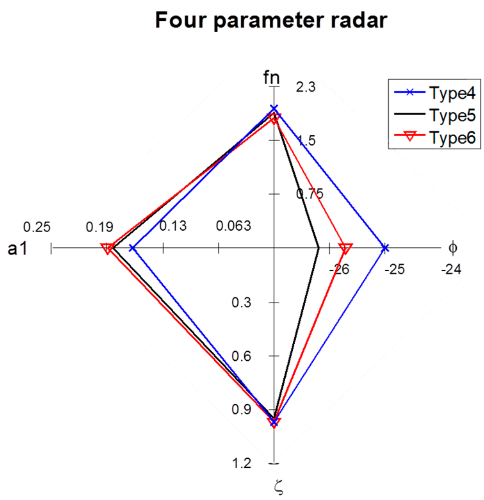

Figure 16. Simulated four-parameter radar charts for impulse steering tests performed using different toe-in angle values.

The phase lag (ϕ) for the Type 4 toe-in angle is better (i.e., lower) than that for the other two angles since the vehicle understeer is enhanced when the initial toe-in angle is negative, indicating that a larger steering wheel angle is required. However, in the impulse steering tests, the vehicle body was required to reach a 0.4 G lateral acceleration within 0.4 s. In other words, the steering wheel angle for the Type 4 toe-in angle increased more rapidly, and the phase lag was smaller. For the Type 6 and Type 5 toe-in angles, the vehicle body should reach the required 0.4 G lateral acceleration at the same steering wheel angle and in the same period of time. The lateral acceleration (0.395 G) for the Type 6 toe-in angle was slightly higher than that for the Type 5 toe-in angle (0.389 G). Consequently, the phase lag for the Type 5 toe-in angle was better (i.e., lower) than that for the Type 5 toe-in angle. Regarding the steady-state yaw rate gain (a_1), Figure 16 shows that the Type 6 toe-in angle resulted in a better steady-state yaw rate gain than the Type 4 or Type 5. This finding is consistent with the results presented previously in Figure 14 and can be attributed to the same reasons as those described in relation to Figures 15 and 16. An inspection of Figure 16 reveals the following observations:

1. The enclosed diamond area for the Type 4 toe-in angle moved towards the top-right corner and, therefore, indicates the occurrence of understeer. By contrast, that for the Type 6 toe-in angle moved towards the bottom-left corner, and therefore indicates the occurrence of oversteer. It is noted that these tendencies are consistent with the results presented in Figure 14 for the yaw rate gain in the constant radius cornering tests.

2. Although the Type 6 toe-in angle appears to result in oversteer, it is not in fact true oversteer but simply oversteer in comparison with the original toe-in angle design (Type 5). Based on an inspection of the radar chart area, the Type 6 toe-in angle actually resulted in a better overall handling performance than the Type 5 design.

5.3. Roll Camber

When the wheel cambers, it moves around the intersection point of the wheel rotation center line and the ground, and the tires deviate from the frontage and roll leftwards and rightwards, respectively, without control. However, the wheels on both sides of the vehicle roll forward together since they are restrained by the front axle. Therefore, a lateral force, F_y, is generated at the wheel center position which pulls the wheels back such that they roll in the same direction. At this point, the contact point between the tire and the ground generates a reaction force, $F_{y\gamma}$, to counter this lateral force. This reaction force is called the roll camber. In the present analysis, the initial camber angle was assigned three different types, namely, Type 7 (−1°), Type 8 (0°), and Type 9 (1°) as shown in Table 13.

Table 13. Camber angle design variables.

Item	Type 7	Type 8	Type 9
Camber angle (°)	−1	0	1

5.3.1. Constant Radius Cornering Test: Yaw Rate Gain (Steady-State Response)

Figure 17 and Table 14 show the simulation results obtained for the yaw rate gain at various vehicle speeds given the three different camber angle values. In general, the results show that the yaw rate gain increased as the camber angle changed from a positive to a negative value.

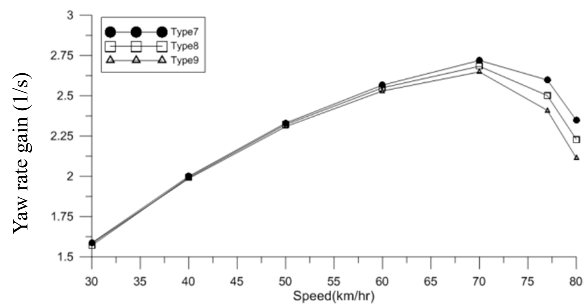

Figure 17. Variation of yaw rate gain with vehicle speed for different initial camber angles.

Table 14. Simulation results for yaw rate gain given different vehicle speeds and camber angles.

Velocity (km/h)	Yaw Rate Gain (Type 7) (1/s)	Yaw Rate Gain (Type 8) (1/s)	Yaw Rate Gain (Type 9) (1/s)
30	1.59	1.57	1.58
40	2.00	1.99	1.98
50	2.33	2.32	2.31
60	2.57	2.55	2.53
70	2.72	2.68	2.65
77	2.60	2.50	2.51
80	2.35	2.23	2.11

The tire slip angle decreases when the camber angle is positive, and, hence, $F_{y\gamma}$ acts in the negative direction. In theory, for a given camber angle, a larger normal force acting on the tire produces a larger roll camber. Thus, when a vehicle performs a curve maneuver, the increased vertical load acting on the off-side wheel due to the load transfer causes the roll camber to increase proportionally. Since the roll camber acts in the opposite direction to the lateral force, the wheel slip angle decreases as the roll camber increases. The lower off-side wheel slip angle prompts a higher slip angle of the nearside wheel. As a result, the vehicle understeers and the yaw rate gain decreases.

5.3.2. Impulse Steering Test: Four-Parameter Radar Plots (Transient-State Response)

Table 15 and Figure 18 show the simulation results obtained for the phase lag, natural frequency, steady-state yaw rate gain, and damping ratio in the impulse steering tests performed using the three different camber angles. It is seen that the steady-state gain and phase lag were relatively insensitive to the camber angle. However, a more significant change in the natural frequency and damping ratio occurs as the camber angle changes from a negative value (Type 7) to a positive value (Type 9). In particular, the natural frequency for the Type 9 camber angle was better (i.e., lower) than that for the Type 7 or Type 8 camber angle, since the understeer coefficient, K_{us}, for Type 9 was higher, and, hence, the yaw rate gain was reduced. Observing Table 15, it is seen that the effects of the camber angle on the damping ratio can be ranked as follows: Type 9 > Type 7 > Type 8. A larger damping ratio gives rise to a more rapid yaw rate gain convergence and, hence, reduces the difference between the steady-state yaw angle gain and the transient-state yaw angle gain. Finally, an inspection of the radar plots in Figure 18 confirms that the effects of the camber angle on the full-vehicle transient handling performance can be ranked as follows: Type 9 > Type 7 > Type 8.

Table 15. Simulation results for impulse steering tests performed using different camber angles.

Item	Phase Lag (ϕ) (°)	Natural Frequency (fn) (Hz)	Steady-State Gain (a1) (1/s)	Damping Ratio (ζ)
Type 7	−25.2334	1.686	0.18309	1.0531
Type 8	−26	1.8825	0.18099	0.9496
Type 9	−24.7735	1.9505	0.17871	1.0775

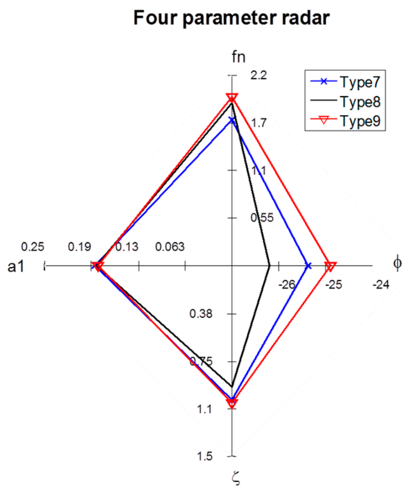

Figure 18. Simulated four-parameter radar charts for impulse steering tests performed using different camber angles.

5.4. Comparison

Tables 16 and 17 summarize the yaw rate gain values obtained in the simulations above for each of the considered design variables (Types 1–9). For each design variable (i.e., the cornering stiffness, toe-in angle, and camber angle), the effects of the considered design changes on the full-vehicle handling performance are quantified by expressing the resulting change in the yaw rate gain as a percentage of the original yaw rate gain. Note that the yaw rate gain was deliberately selected as the comparative parameter here, since its value reflects the interaction of the entire chassis system including the suspension system, the steering system, and the tire system. Overall, the results show that the vehicle cornering handling sensitivity can be improved by increasing the cornering stiffness, increasing the initial toe-in angle, and reducing the initial camber angle.

Table 16. Effects of changes in steady-state design variables on vehicle handling performance.

Item	Design Variable	Yaw Rate Gain (Steady State)	Percentage (Steady State)
Type 1 (original)	Cornering stiffness (original value)	2.68	0%
Type 2	Cornering stiffness (increased by 30%)	3.22	20%
Type 3	Cornering stiffness (decreased by 30%)	2.21	−17%
Type 4	Initial toe-in angle (−1°)	2.35	−12.3%
Type 5 (original)	Initial toe-in angle (0°)	2.68	0%
Type 6	Initial toe-in angle (1°)	3.07	9.7%
Type 7	Initial camber angle (−1°)	2.72	1.47%
Type 8 (original)	Initial camber angle (0°)	2.68	0%
Type 9	Initial camber angle (1°)	2.65	−1.11%

Table 17. Effects of changes in transient-state design variables on vehicle handling performance.

Item	Design Variable	Yaw Rate Gain (Transient)	Percentage (Transient)
Type 1 (original)	Cornering stiffness (original value)	0.18099	0%
Type 2	Cornering stiffness (increased by 30%)	0.19171	5.92%
Type 3	Cornering stiffness (decreased by 30%)	0.14356	−20.7%
Type 4	Initial toe-in angle (−1°)	0.15898	−12.2%
Type 5 (original)	Initial toe-in angle (0°)	0.18099	0%
Type 6	Initial toe-in angle (1°)	0.1871	3.38%
Type 7	Initial camber angle (−1°)	0.18309	1.16%
Type 8 (original)	Initial camber angle (0°)	0.18099	0%
Type 9	Initial camber angle (1°)	0.17871	−1.26%

6. Conclusions

This study investigated the full-vehicle handling performance of a commercial vehicle fitted with an SLA strut front suspension system and a multi-link rear suspension system. Based on a detailed inspection of the hardpoint positions of the suspension system and steering system, a full-vehicle ADAM analysis model was constructed and used to evaluate the handling performance of the vehicle in simulated constant radius cornering tests and impulse steering tests, respectively. The corresponding steady-state and transient-state responses of the vehicle were confirmed by experimental tests. The validated model was then used to investigate the design parameters which dominated the understeer behavior of the vehicle and the effects of the three main design variables (namely, the cornering stiffness, the toe-in angle, and the camber angle) on the steady-state and transient-state vehicle handling performance. In general, the results showed that the suspension system factors affecting the understeer performance (K_{us}) can be ranked in terms of decreasing effect as follows: cornering stiffness >lateral force compliance steer >roll steer >roll camber >aligning torque. Moreover, the cornering handling performance can be improved by increasing the cornering stiffness and initial toe-in angle and reducing the initial camber angle.

Author Contributions: H.-H.H. and M.-J.T. conceived of the presented idea. We developed the theory and M.-J.T. performed the CAE. H.-H.H. verified the analytical methods and supervised the findings of this work. All authors discussed the results and contributed to the final manuscript.

Funding: The authors gratefully acknowledge the financial support provided to this study by the Ministry of Science and Technology, R.O.C.

Conflicts of Interest: The authors declare no conflict of interest.

Nomenclature

Symbol	Designation	Unit
δ_f, δ_r	Front/rear tire steering angle	°
L	Wheelbase	m
L_f, L_r	Distance from CG to front/rear axle	m
R	Cornering radius	m
K_{us}	Understeer coefficient	–
W_f, W_r	Front/rear tire vertical load	N
V_x	Longitudinal velocity	m/s
V_y	Lateral velocity	m/s
I_z	Polar moment of inertia	mm^4
ω_n	Natural frequency	Hz
$C_{\alpha f}$, $C_{\alpha r}$	Front/rear tire cornering stiffness	N/rad
g	Acceleration of gravity	m/s^2
Ω_z	Yaw velocity	°/s
A_y	Lateral acceleration	G
F_{yf}, F_{yr}	Front/rear tire lateral force	N
m	Mass	kg
δ_A	Ackerman steering angle	°
α_f, α_r	Front/rear tire slip angle	°
δ_{SW}	Steering wheel angle	°
ζ	Damping ratio	*

References

1. Holdmann, P.; Köhn, P.; Möller, B. *Suspension Kinematics and Compliance—Measuring and Simulation*; Paper No. 980897; SAE International: Warrendale, PA, USA, 1998.
2. Dixon, J.C. *Suspension Geometry and Computation*; Wiley: Hoboken, NJ, USA, 2009; pp. 99–125.
3. Mitchell, W.; Staniforth, A.; Scott, I. *Analysis of Ackermann Steering Geometry*; Paper No. 2006-01-3638; SAE International: Warrendale, PA, USA, 2006.
4. Wang, X.F.; Hu, T.; Jin, X.H.; Li, D.M.; Hou, Y.J. Experimental Study on Relationship between Inside and Outside Steered Wheels of Motor Vehicle. *Tract. Farm Transp.* **2010**, *37*, 13–15.
5. Upadhyay, V.; Pathak, A.; Kshirsagar, A.; Khan, I. *Development of Methodology for Steering Effort Improvement for Mechanical Steering in Commercial Vehicles*; Paper No. 2010-01-1887; SAE International: Warrendale, PA, USA, 2010.
6. Singh, S.; Hiremath, V.; Ojha, V.; Jadhav, N. *Effect of Steering System Compliance on Steered Axle Tire Wear*; Paper No. 2012-01-1909; SAE International: Warrendale, PA, USA, 2012.
7. Azadi, S.; Mirzadeh, O. *Sensitivity Analysis of Steering System Parameters for a Passenger Car by DOE Method*; Paper No. 2005-01-1277; SAE International: Warrendale, PA, USA, 2005.
8. Guvenc, B.A.; Acarman, T.; Guvenc, L. Coordination of Steering and Individual Wheel Braking Actuated Vehicle Yaw Stability Control. In Proceedings of the Intelligent Vehicle Symposium, Columbus, OH, USA, 9–11 June 2003; pp. 288–293.
9. Nagai, M.; Shino, M.; Gao, F. Study on integrated control of active front steering angle and direct yaw moment. *JSAE Rev.* **2002**, *23*, 309–315. [CrossRef]
10. You, S.; Jo, J.; Yoo, S.; Hahn, J.; Lee, K. Vehicle Lateral Stability Management using Gain-Scheduled Robust Control. *J. Mech. Sci. Technol.* **2006**, 1898–1913. [CrossRef]
11. Cho, W.; Heo, H.; Yi, K. An investigation into unified chassis control for agility, maneuverability and lateral stability. In Proceedings of the 14th International IEEE Conference on Intelligent Transportation Systems (ITSC), Washington, DC, USA, 5–7 October 2011; pp. 949–955.
12. Mimuro, T.; Ohsaki, M.; Yasuna, H.; Satoh, K. *Four Parameter Evaluation Method of Lateral Transient Response*; Paper No. 901734; SAE International: Warrendale, PA, USA, 1990.
13. Gillespie, T.D. *Fundamentals of Vehicle Dynamics*; Society of Automotive Engineers Inc.: Warrendale, PA, USA, 1992; pp. 217–226.

14. MD. *Adams, Online Help: Chassis Appendix, MSC*; Software Corporation: Beijing, China, 2010; pp. 332–334.
15. Heißing, B.; Ersoy, M. *Chassis Handbook*; Vieweg+Teubner Verlag: Berlin, Germany, 2011; pp. 354–355.

© 2019 by the authors. Licensee MDPI, Basel, Switzerland. This article is an open access article distributed under the terms and conditions of the Creative Commons Attribution (CC BY) license (http://creativecommons.org/licenses/by/4.0/).